Combustion and Flame 185 (2017) 220–233

Contents lists available at ScienceDirect

Combustion and Flame

journal homepage: www.elsevier.com/locate/combustflame

Fuel-rich n-heptane oxidation: A shock tube and laser absorption study

Zachary E. Loparo[a], Joseph G. Lopez[a], Sneha Neupane[a], William P. Partridge Jr.[b], Konstantin Vodopyanov[c], Subith S. Vasu[a,*]

[a] Center for Advanced Turbomachinery and Energy Research (CATER), Mechanical and Aerospace Engineering, University of Central Florida, Orlando, FL, USA
[b] Fuels, Engines, and Emissions Research Center (FEERC), National Transportation Research Center, Oak Ridge National Laboratory, Knoxville, TN, USA
[c] CREOL, The College of Optics and Photonics, University of Central Florida, Orlando, FL, USA

ARTICLE INFO

Article history:
Received 22 March 2017
Revised 23 June 2017
Accepted 14 July 2017

Keywords:
Shock tube
n-Heptane
Laser absorption
Fuel rich
Chemical kinetics

ABSTRACT

The chemical kinetics of n-heptane (n-C_7H_{16}) – an important reference compound for real fuels – oxidation are well studied at stoichiometric and lean conditions. However, there is only limited information on the n-heptane chemical kinetics in fuel-rich combustion. In order to verify the accuracy of chemical kinetic models at these conditions, the oxidation of rich n-heptane mixtures has been investigated. Combustion of n-C_7H_{16}/O_2/Ar mixtures at equivalence ratios, φ, of 2.0 and 3.0 behind reflected shock waves has been studied at temperatures ranging from 1066 to 1502 K and at pressures ranging from 1.4 to 6.2 atm. Reaction progress was monitored by recording pressure and absorption time-histories of ethylene (C_2H_4) and n-heptane at a location 2 cm from the endwall of a 14-cm inner diameter shock tube. Ethylene and n-heptane absorption time-histories were measured, respectively, using absorption spectroscopy at 10.532 μm from a tunable CO_2 laser and at around 3.4 μm from a continuous wave distributed feedback interband cascade laser (ICL). The measured absorption time-histories were compared with modeled predictions from the Lawrence Livermore National Lab (LLNL) detailed n-heptane reaction mechanism. To the best of our knowledge, current data are the first time-resolved n-heptane and ethylene concentration measurements conducted in a shock tube at these conditions.

1. Introduction

Recent research has pursued the combustion and performance advantages of in-cylinder reforming processes where fuel is injected into O_2-deficient engine operating conditions, to convert a portion of the fuel into products containing significant levels of small-chained partially-oxidized hydrocarbons. The presence of reformate can extend knock limit and dilution tolerance of SI combustion [1,2]. By exploiting the properties of reformate with well-understood engine technologies, such as dilute SI combustion and compression ratio, light-duty vehicle fuel economy can be increased towards legislated fuel economy mandates (e.g., CAFE 2025 [3]). One such method is fuel injection in the negative valve overlap (NVO) period in order to convert a portion of the fuel into short-chain hydrocarbons (e.g., ethylene) by partial oxidation and thermal cracking. These products may then be used to control the combustion properties of the fuel and air mixture introduced into the other cylinders [4]. In an NVO environment, the mixture within the cylinder is often fuel-rich [2]. Other strategies known as spark-assisted HCCI (SA-HCCI) and spark assisted compression ignition (SACI) have been pursued as well [5]. In this case, HCCI heat release is obtained after a stoichiometric NVO assisted by spark initiation. The recent dedicated exhaust gas recirculation strategy (D-EGR) [6] uses one of cylinders to produce a reformate and can result in fuel savings of up to 10%. Fuel rich conditions also exist in other common combustion environments, such as diesel engine sprays and in aircraft gas turbines.

It has been found that the concentration of reformate species is strongly dependent on the injected fuel type and the time available for reactions [7,8]. Surprisingly, a comparison of species concentrations obtained during NVO reformate experiments including hydrogen (H_2), acetylene (C_2H_2), and ethylene (C_2H_4) and those predicted with recent Lawrence Livermore National Labs (LLNL) mechanisms [9–11] did not match [4]. The model predictions failed to capture the experimental trend of increased reformate concentrations with advanced fuel injection timings. Thus, a detailed understanding of the fuel chemistry that occurs during engine relevant oxygen deficient conditions is warranted.

* Corresponding author.
E-mail address: subith@ucf.edu (S.S. Vasu).

http://dx.doi.org/10.1016/j.combustflame.2017.07.016
0010-2180/

Table 1
Summary of experimental conditions and species diagnostics used in n-heptane oxidation studies in shock tubes.

Study	Year	Pressure (atm)	Temperature (K)	Fuel loading	Equivalence ratio (φ)	Species Diagnostics
This work	2017	1.4–1.9, 4.8–6.2	1066–1502	2%	2.0, 3.0	n-heptane: 3.403 µm ethylene: 10.532 µm
Tekawade et al. [34]	2016	10	686–1290	0.05–0.5%	1.0	CO: 4.59 µm
Campbell et al. [33]	2015	6.1–7.4	651–823	1%	0.75	n-heptane: 3.93 µm OH, CH_2O: 306.7 nm CO_2: 4.2 µm H_2O:2.5 µm OH^*: emission
Zhang et al. [13]	2013	2, 10	1200–1500	0.38%	1.0	CH^*: emission
Pyun et al. [14]	2013	1.5	1200–1600	1%	Pyrolysis	CH_4: 3.43 µm ethylene: 10.532 µm
Pilla et al. [40]	2011	1.3–3.3	1350–1950	300 ppm	Pyrolysis	ethylene: 10.532 µm
Davidson et al. [20]	2010	2	1300–1600	300 ppm	1.0	n-heptane: 3.39 µm ethylene: 10.532 µm OH: 306.5 nm CO_2: 2.7 µm H_2O: 2.5 µm
Shen et al. [41]	2009	9–58	786–1396	0.5–1.8%	0.25, 0.5, 1.0	OH^*: emission
Vasu et al. [21]	2009	15	1121–1332	750–1000 ppm	0.5	OH: 306.5 nm
Davidson et al. [29]	2007	1.6–2.0	1100–1560	100–500 ppm	1, pyrolysis	CH_3: 216 nm
Smith et al. [32]	2005	2	1500–1650	0.40%	0.5, 1.0, 2.0	CH^*, OH^*: emission
Herzler et al. [42]	2005	50	720–1100	0.2–0.7%	0.1–0.4	CH^*: emission
Gauthier et al. [30]	2004	12–25, 45–60	850–1280	1.87%	0.5, 1.0, 2.0	CH^*, OH^*: emission
Davidson et al. [28]	2001	2.0–3.8	1357–1784	300 ppm	0.8–1.2	OH: 306.5 nm
Ciezki et al. [25]	1993	3.2–41	660–1350	0.9–5.5%	0.5–3.0	CH^*: emission

n-Heptane is a component of primary reference fuel for both diesel and gasoline, and is one of the most well studied fuels especially at stoichiometric and lean conditions [12–26]. However, there is a lack of rich n-heptane combustion studies in the literature, and those that do investigate rich mixtures do not provide concentration time-histories of intermediate species [20,21,25,27–34]. Ethylene has been shown to be produced in significant quantities during fuel-rich n-heptane combustion and is therefore of high importance for mechanism development [12,21,35]. The use of non-intrusive, laser-based diagnostics in shock tubes enables in-situ measurements of species concentration time-histories and reaction rates with high temporal resolution. Concentration time-history data from shock tubes offers rich targets for chemical kinetic model development and validation when compared to ignition delay time data or endpoint species measurements provided by gas chromatograph (GC/MS) techniques [17,36–38].

In this work, time-histories of ethylene and n-heptane absorbances were measured at pressure ranges from 1.4 to 6.2 atm over a temperature range of 1066 to 1502 K with mixtures of n-heptane and oxygen in an argon bath at equivalence ratios (φ) of 2.0 and 3.0 and with initial n-heptane concentration of 2% behind reflected shock waves. This work is an extension of previous experiments, detailed in [39]. Results were compared to the predictions of LLNL detailed heptane chemical kinetic mechanism, which has not been validated at equivalence ratios of above 1.0 [11]. A summary of the conditions and diagnostics used in this and previous work performed in shock tubes is provided in Table 1.

To the best of our knowledge, current data are the first time-resolved n-heptane and ethylene concentration measurements conducted in a shock tube at these conditions of high fuel loading, rich mixtures, and over a wider pressure range than previously investigated.

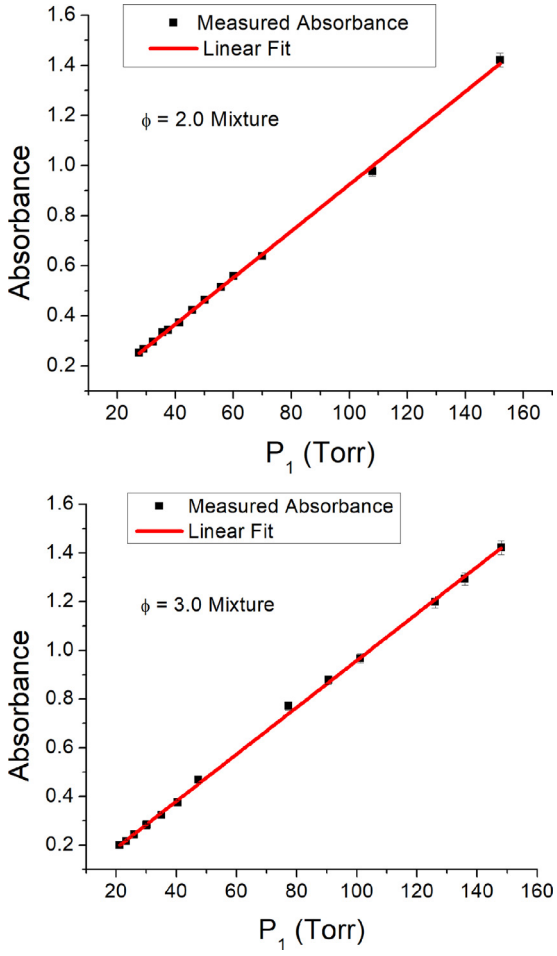

Fig. 1. Measured absorbance at 3.4 μm versus initial mixture pressure in the shock tube across multiple tests.

2. Experimental procedure

2.1. Shock tube facility

Experiments were performed in a stainless steel, heated shock tube located at the University of Central Florida (UCF) with an inner diameter of 14 cm. The details of the shock tube facility are in Refs. [43-46] and only a brief description is provided here. The shock tube facility with double diaphragm configuration is designed for producing pressures ranging from 1 to 90 atm and temperatures ranging from 600 to 4000 K. In the current work, a single diaphragm configuration was utilized; the diaphragms were 0.127 mm and 0.381 mm thick in order to achieve test pressures (P_5) ranging from 1.4 to 1.9 atm and 4.8 to 6.2 atm, respectively.

All measurements were performed at a test section located 2 cm away from the endwall of the driven section, which has eight optical access ports. A Kistler 603B1 piezoelectric pressure transducer with Room Temperature Vulcanization (RTV) silicone coating was installed in one access port to measure pressure in the reflected shock region. A pair of sapphire windows, 3 mm thick

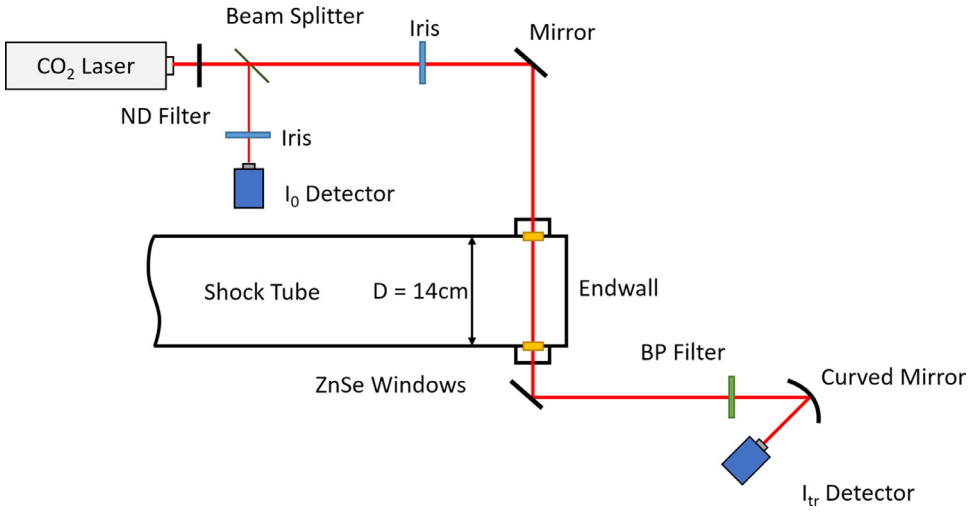

Fig. 2. Schematic of the end section of the shock tube with the laser and optical components at a 2 cm sidewall location. (BP: bandpass filter, ND: neutral density filter).

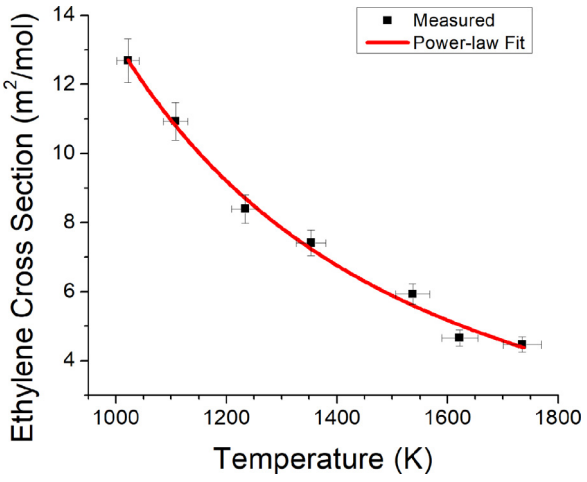

Fig. 3. Measured ethylene absorption cross section as a function of temperature for P = 1.4–1.9 atm. The curve is the power-law fit described by Eq. (2).

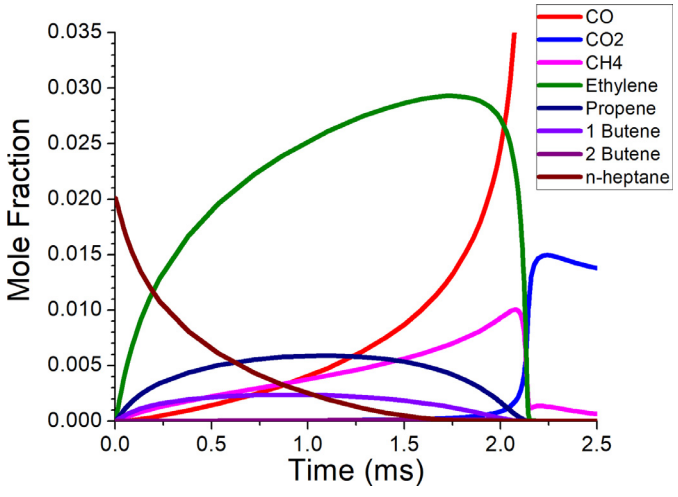

Fig. 5. Predicted time-histories for major species during the combustion of a φ = 2 n-heptane mixture at T_5 = 1235 K and P_5 = 1.8 atm. Ethylene is formed in much larger concentrations than possible interfering species (simulations using detailed LLNL n-heptane mechanism [11] with Chemkin Pro [51]).

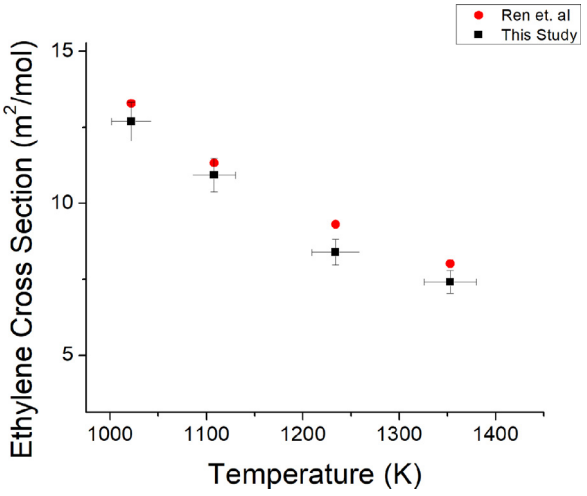

Fig. 4. Comparison of measured ethylene cross section and that given by the temperature and pressure dependent fit of Ren et al. [50] over the range of temperatures studied in experiments with pressures from 4.8 to 6.2 atm.

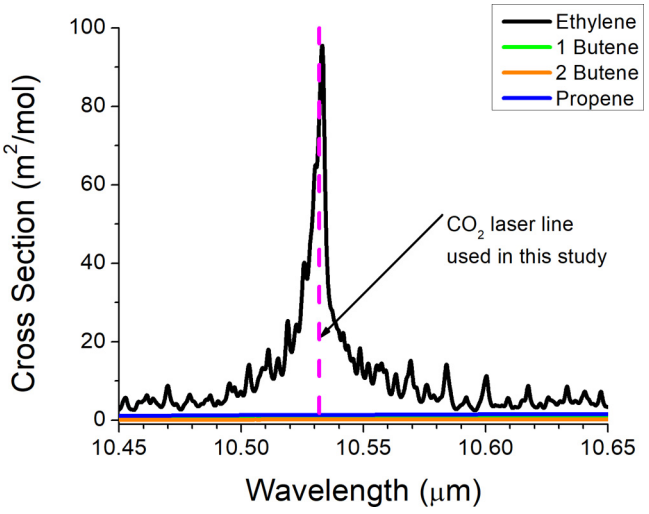

Fig. 6. The CO_2 P14 line at 10.532 μm overlaps with a strong absorption feature of ethylene with little influence from other possible interfering species (wavelength selection at room temperature from PNNL [49]).

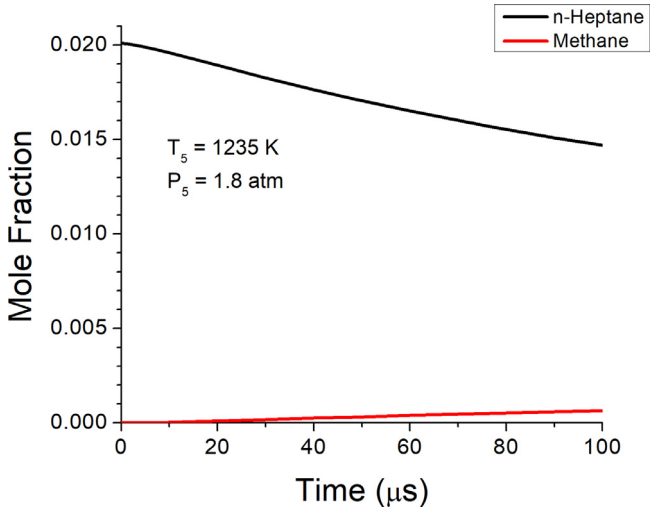

Fig. 7. Modeled concentration time-histories for n-heptane (black) and methane (red) at $T = 1235$ K and $P = 1.8$ atm (simulations using detailed LLNL n-heptane mechanism [11] with Chemkin Pro [51]). (For interpretation of the references to color in this figure legend, the reader is referred to the web version of this article).

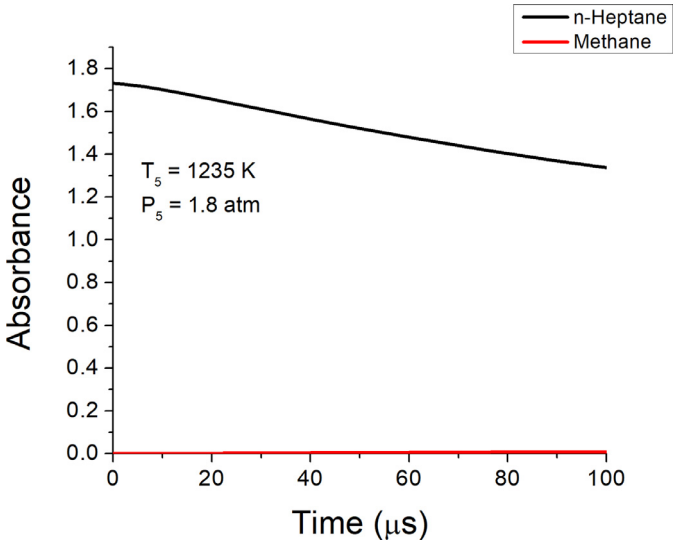

Fig. 8. Predicted n-heptane and methane absorbance signals for $T = 1235$ K experiment (HITRAN [48]). At early times, the absorption of heptane dominates and interference from methane is negligible, and thus the measured signal is primarily due to n-heptane. (Simulations using detailed LLNL n-heptane mechanism [11] with Chemkin Pro [51]).

and 19.05 mm in diameter, was mounted in opposing optical ports to allow for line of sight measurement of n-heptane time-histories using a 3.4 μm laser. A separate pair of wedged ZnSe windows, 3 mm thick and 12.7 mm in diameter, were mounted in opposing ports for line of sight absorption measurements with a CO_2 laser at 10.532 μm for measuring ethylene time-histories. Two 8-channel data acquisition boards (NI PCI-6133, 2.5 MS/second/channel) were used to measure pressure and laser absorption time-histories at a rate of 2 MHz. Four piezoelectric pressure transducers (PCB113B26, 500 kHz frequency response), connected to three time interval counters (Agilent 53220A, 0.1 ns time resolution), were placed along the last 1.4 m of the shock tube to measure incident shock velocity, which was then linearly extrapolated to the endwall. Temperature and pressure (T_5 and P_5) in the reflected shock region are calculated based on the extrapolated shock velocity and the initial temperature and pressure (T_1 and P_1) in the test section using one dimensional shock relations, assuming chemically frozen,

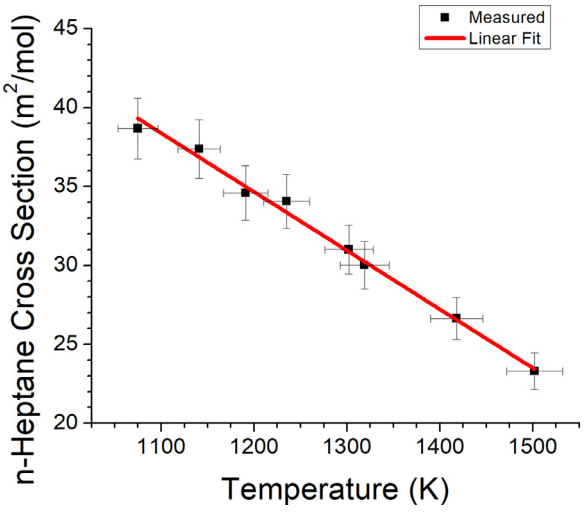

Fig. 9. Measured n-heptane absorption cross section as a function of temperature. The cross section is fit with a line over the temperature range used in this study.

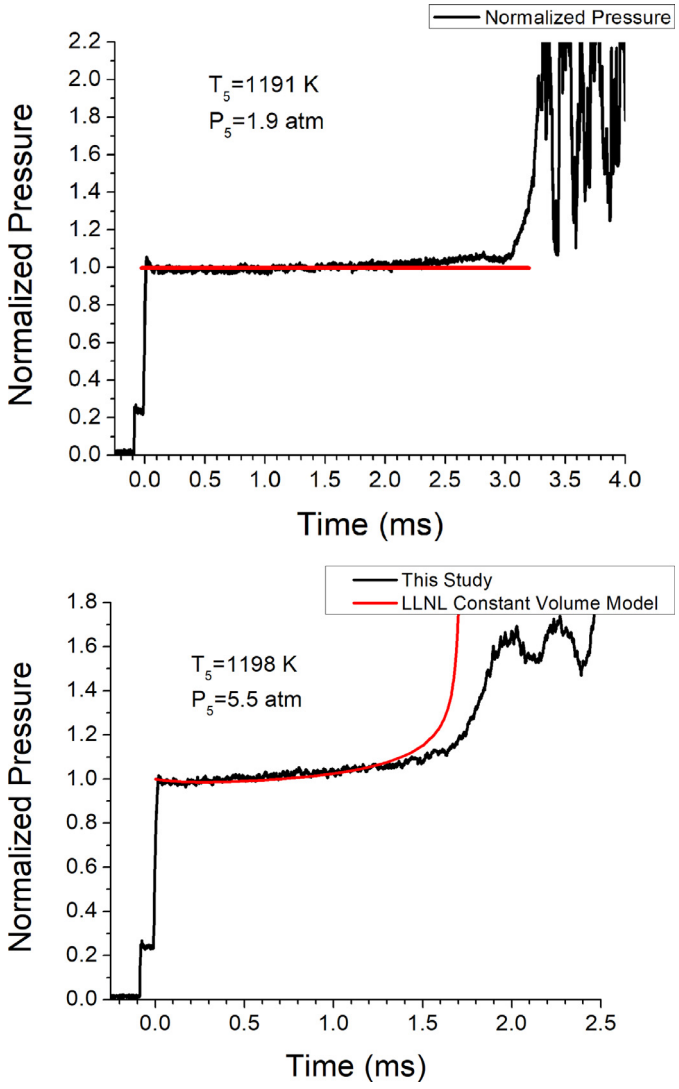

Fig. 10. Pressure time histories for experiments displaying constant pressure (top) and constant volume (bottom) behavior (simulations using detailed LLNL n-heptane mechanism [11] with Chemkin Pro [51]).

Table 2
Summary of experimental conditions.

P_5 (atm)	T_5 (K)	$X_{n\text{-}C7H16}$ (%)	X_{O2} (%)	X_{Ar} (%)	ϕ	Modeling assumption
1.9	1075	2.0	11.0	87.0	2.0	Const. HP
1.9	1141	2.0	11.0	87.0	2.0	Const. HP
1.9	1191	2.0	11.0	87.0	2.0	Const. HP
1.8	1235	2.0	11.0	87.0	2.0	Const. HP
1.7	1302	2.0	11.0	87.0	2.0	Const. HP
1.6	1319	2.0	11.0	87.0	2.0	Const. HP
1.7	1418	2.0	11.0	87.0	2.0	Const. HP
6.2	1066	2.0	11.0	87.0	2.0	Const. UV
6.0	1114	2.0	11.0	87.0	2.0	Const. UV
5.7	1179	2.0	11.0	87.0	2.0	Const. UV
5.5	1244	2.0	11.0	87.0	2.0	Const. UV
1.6	1132	2.1	7.7	90.2	3.0	Const. HP
1.6	1233	2.1	7.7	90.2	3.0	Const. UV
1.5	1249	2.1	7.7	90.2	3.0	Const. UV
1.5	1375	2.1	7.7	90.2	3.0	Const. UV
1.4	1438	2.1	7.7	90.2	3.0	Const. UV
1.4	1502	2.1	7.7	90.2	3.0	Const. UV
5.9	1140	2.1	7.7	90.2	3.0	Const. UV
5.6	1157	2.1	7.7	90.2	3.0	Const. UV
5.5	1198	2.1	7.7	90.2	3.0	Const. UV
5.2	1302	2.1	7.7	90.2	3.0	Const. UV
5.0	1356	2.1	7.7	90.2	3.0	Const. UV
4.8	1454	2.1	7.7	90.2	3.0	Const. UV

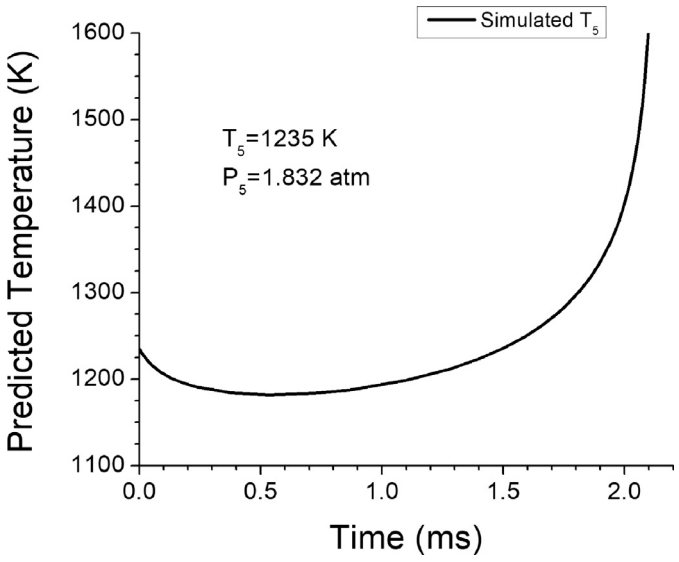

Fig. 11. Simulated temperature time history for $\varphi = 2.0$, 2% mixture of n-heptane in oxygen and argon. The temperature changes by over 30% over the course of the experiment (simulations using detailed LLNL n-heptane mechanism [11] with Chemkin Pro [51]).

vibrationally equilibrated gases. Incident shock attenuation was typically less than 1%, and the uncertainty in reflected shock temperature and pressure were estimated to be less than ± 2% and ± 3%, respectively. The primary source of uncertainty in temperature and pressure is uncertainty in the reflected shock velocity, based on timer counter measurements.

2.2. n-Heptane/O_2/Ar mixture preparation

Before mixture preparation and shock tube tests, the shock tube and mixing tank facilities were vacuumed by rotary vane pumps (Agilent DS102) and a turbomolecular pump (Agilent V301). Vacuum pressures were measured by a convection gauge (Lesker KJL275804LL) and an ionization gauge (Lesker KJLC354401YF) operating between 1000 and 1×10^{-4} Torr and between 5×10^{-2} and 1×10^{-9} Torr, respectively. The shock tube was vacuumed to 5×10^{-5} Torr before each experiment was conducted, taking typically 45 min.

The shock tube facility has two (each 33 L) Teflon-coated stainless steel high purity mixing facilities and test gas mixtures were prepared manometrically in one of them. The mixing tank was heated to 120 °C using a custom-designed heating jacket before preparation of mixtures to ensure that no fuel condensed on the walls. Partial pressures were measured with 100 Torr- and 10,000 Torr-full scale range baratrons (MKS Baratron E27D and 628D, accuracies of 0.12% and 0.25% of reading, respectively). Research grade (purity> 99.999%) gases (Ar, O_2) from Praxair and n-heptane (> 99%, Fisher Scientific) were used to prepare mixtures with equivalence ratio $\varphi = 2.0$ and 3.0, and 2% n-heptane initial mole fraction. During preparation, n-heptane was introduced into the mixing tank and was allowed to fully vaporize, which usually took approximately 30 min. Oxygen was preheated to 120 °C to match the mixing tank temperature before being introduced. By preheating oxygen, condensation of n-heptane was prevented and the desired equivalence ratio was achieved. Argon was then introduced into the mixing tank without pre-heating until the mixture was diluted to 2% n-heptane. Argon was used as a bath gas in order to minimize non-idealities such as reflected shock bifurcation that occur with high concentrations of polyatomic molecules in the driven gas mixture [47]. Though practical engines use N_2 as the diluent, chemical kinetic simulations showed that there are only small differences between the chemical kinetics of n-heptane oxidation in argon and nitrogen baths. The mixtures were left to mix for at least six hours before any shock tube experiments were performed.

It is very important to accurately characterize mixtures made with liquid fuels due to their tendency to condense. Hence the mole fraction of n-heptane in the mixture was verified by laser absorption at 3.4 μm (details in the next section) during shock tube filling, as shown in Fig. 1, and found to be 2.02 ± 0.08% (95%CI) for the $\varphi = 2.0$ mixture and 2.10 ± 0.10% (95%CI) for the $\varphi = 3.0$ mixture.

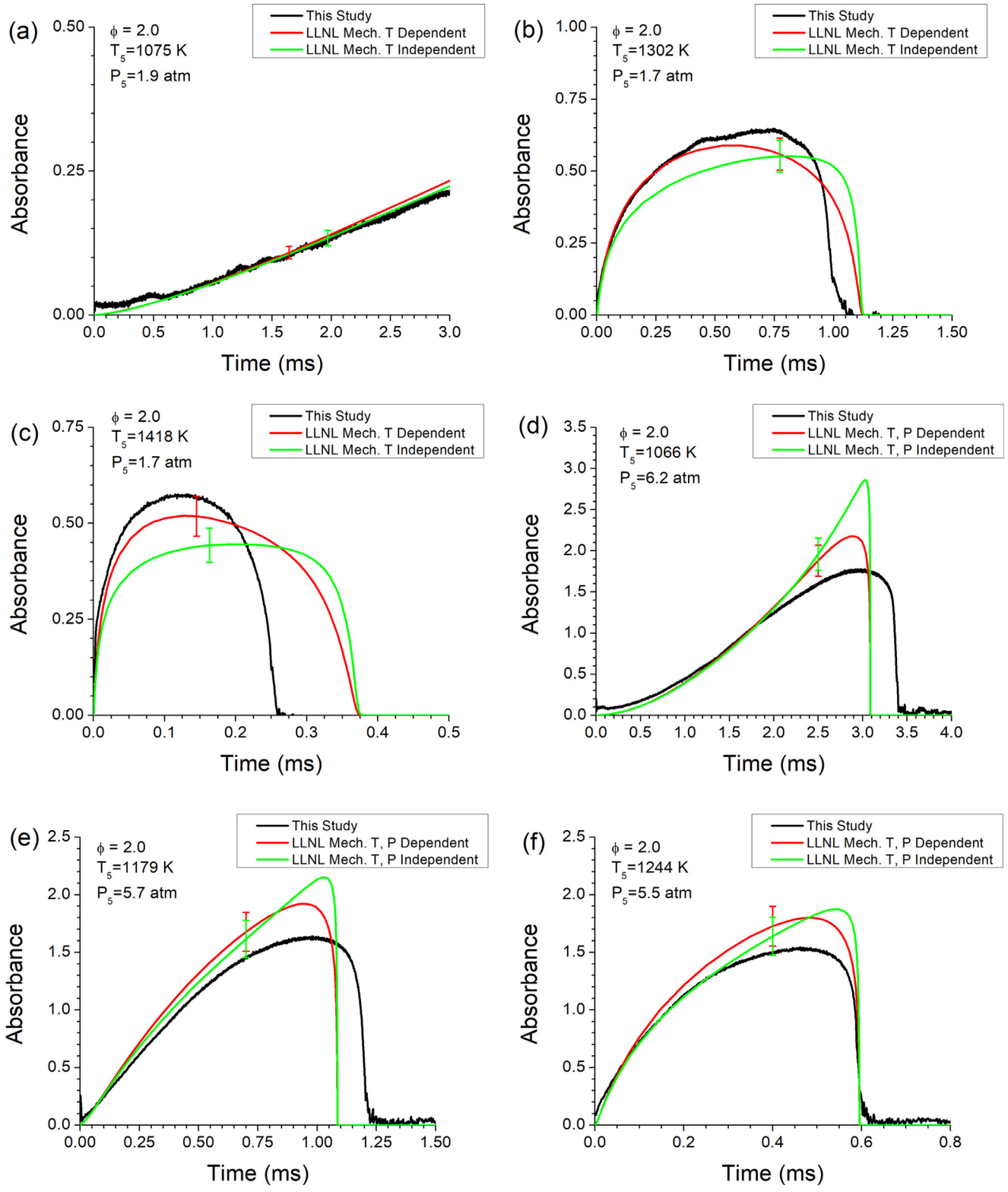

Fig. 12. Absorbance time-histories for ethylene. (a–c) $\varphi = 2.0$, $P \cong 1.8$ atm. (d–f) $\varphi = 2.0$, $P \cong 5.8$ atm. (g–i) $\varphi = 3$, $P \cong 1.5$ atm. (j–l) $\varphi = 3.0$, $P \cong 5.3$ atm. Black traces are measured absorbance. Red traces are the modeled absorbance assuming time dependent temperature and pressure (Rule 1). Green traces are the modeled absorbance assuming constant temperature and pressure over the course of the experiment, with the only variance in absorbance being due to ethylene mole fraction (Rule 2). Simulations were performed using the detailed LLNL n-heptane mechanism [11] with Chemkin Pro [51]. (For interpretation of the references to color in this figure legend, the reader is referred to the web version of this article).

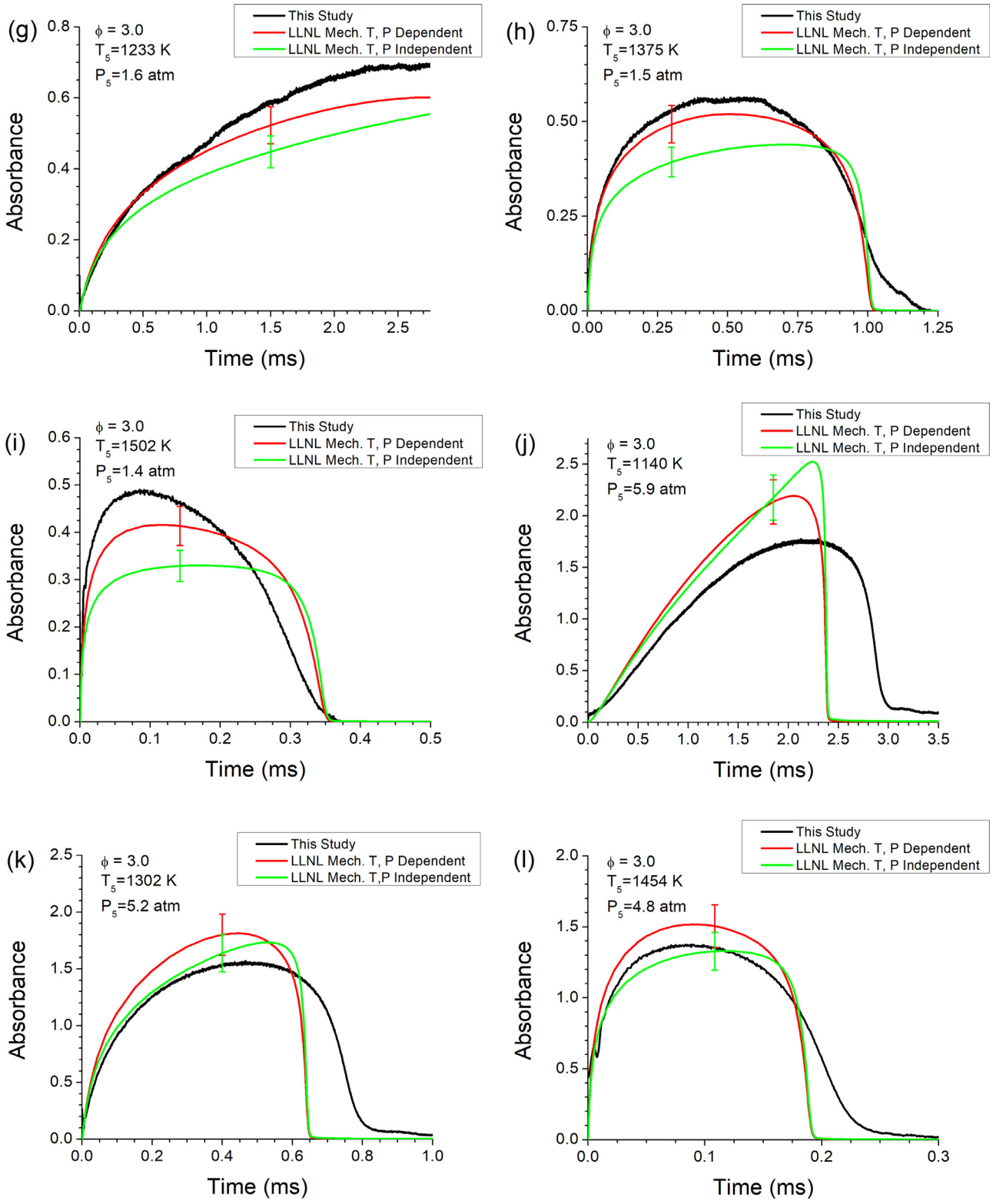

Fig. 12. Continued

2.3. Ethylene and n-heptane laser absorption time-history measurements

2.3.1. Ethylene laser scheme

Ethylene time-histories were measured via direct absorption spectroscopy using a tunable CO_2 gas laser (Access Laser L4GS). The optical setup for this diagnostic is schematically shown in Fig. 2.

The laser was more powerful than necessary for making absorption measurements, so its output intensity was reduced with a neutral density filter of optical density 1. The beam was then split into a reference beam and a signal beam by a 50/50 beam

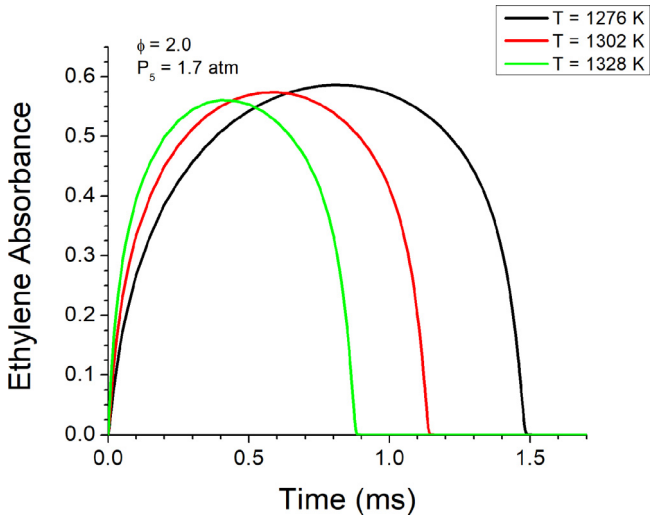

Fig. 13. Modeled ethylene absorbance time-histories for a $\varphi = 2.0$ mixture at constant pressure $P_5 = 1.7$ atm with the temperature T_5 varied by ± 2% from 1302 K. The variance in T_5 leads to a variance of approximately 30% in the time until rapid ethylene consumption.

splitter. Irises were used after the beam splitter to control the intensity of the light incident on the detectors. The intensity of the reference beam (I_0) was measured with a thermoelectrically cooled photovoltaic detector (Vigo PVI-3TE-10.6) and used to monitor laser power output fluctuations over the course of the experiment. The transmitted beam (I_{tr}) was transmitted through the ZnSe windows in the shock tube before being filtered by a bandpass filter to reduce interference on the detector due to emissions of gas species at high temperature. The filtered transmitted beam was incident on a focusing mirror which reflected it onto a second identical photovoltaic detector, effectively increasing the detector area size and mitigating beam steering effects.

The observed absorbance of the laser is related to the mole fraction of ethylene by the Beer–Lambert law, as shown in Eq. (1):

$$\alpha_\lambda = -\ln\left(\frac{I_{tr}}{I_o}\right)_\lambda = \sigma(\lambda, T, P)\frac{P_{tot}}{RT}xL, \tag{1}$$

where α_λ is the absorbance, I_{tr} is the transmitted intensity, I_0 is the reference intensity, σ is the absorption cross section (cm^2/mol), P_{tot} is the total pressure (atm), T is the temperature (K), R is the ideal gas constant (cm^3 atm/mol K), x is the mole fraction of the absorbing species, and L is the optical path length (cm).

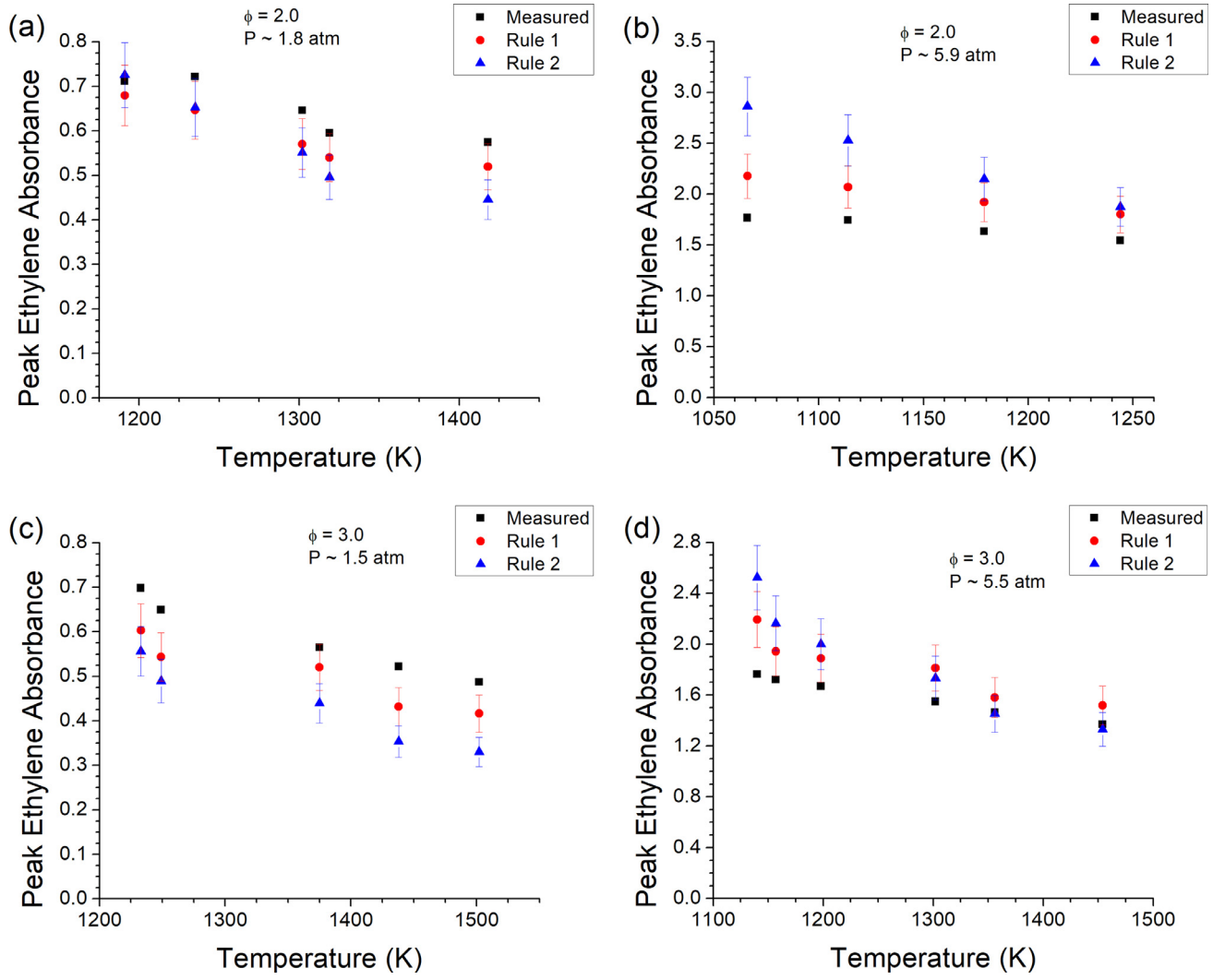

Fig. 14. Peak ethylene absorbance, defined as the maximum value of measured or simulated absorbance obtained. Experiments in which ethylene concentration does not reach a maximum and subsequently decrease during the test time are omitted.

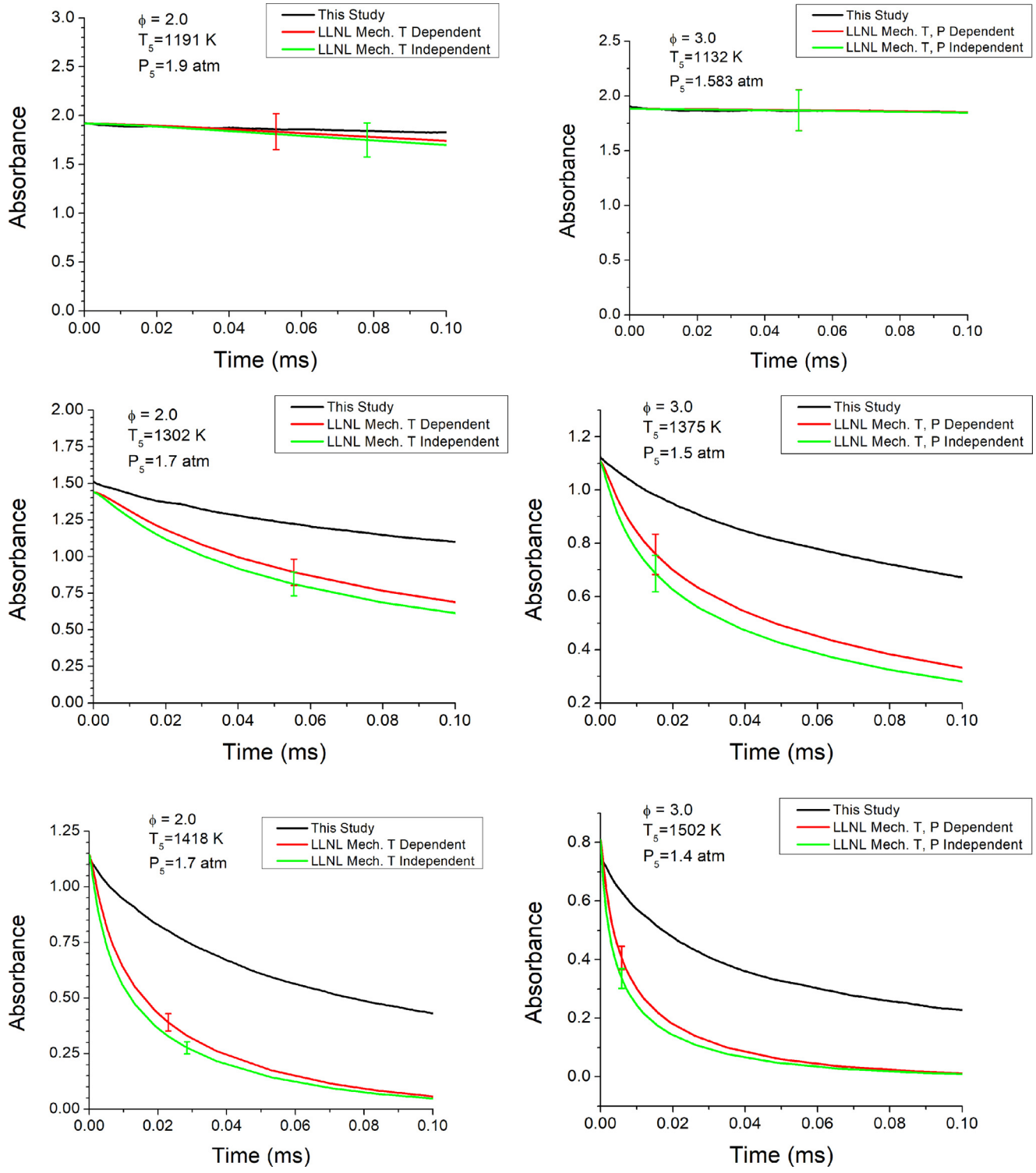

Fig. 15. Comparison of measured and simulated absorbance time histories due to n-heptane concentration for the first 100 µs of selected experiments over several conditions for both $\varphi = 2.0$ and $\varphi = 3.0$ mixtures (simulations using detailed LLNL n-heptane mechanism [11] with Chemkin Pro [51]). Black traces are measured absorbance. Red traces are the modeled absorbance assuming time dependent temperature and pressure (Rule 1). Green traces are the modeled absorbance assuming constant temperature and pressure over the course of the experiment, with the only variance in absorbance being due to ethylene mole fraction (Rule 2). Only traces from low pressure experiments are included, as the 3.4 µm signal is saturated for high pressure experiments. (For interpretation of the references to color in this figure legend, the reader is referred to the web version of this article).

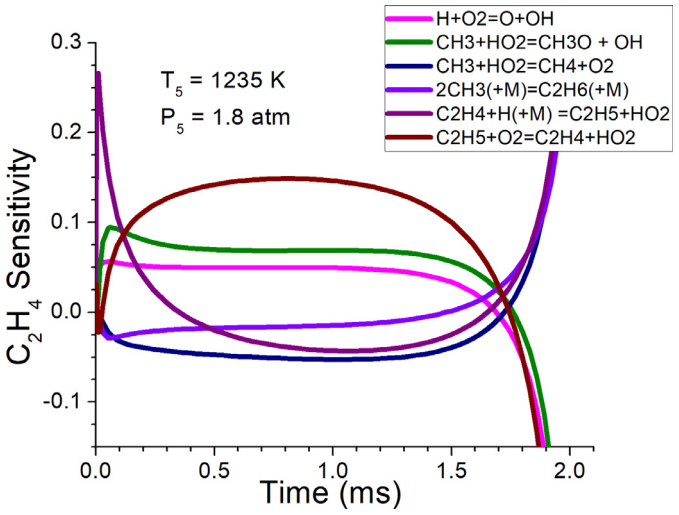

Fig. 16. Sensitivity analysis results for ethylene formation. The dominant reaction responsible for the formation of n-heptane during the majority of its residence period is $C_2H_5 + O_2 = C_2H_4 + HO_2$ (simulations using detailed LLNL n-heptane mechanism [11] with Chemkin Pro [51]).

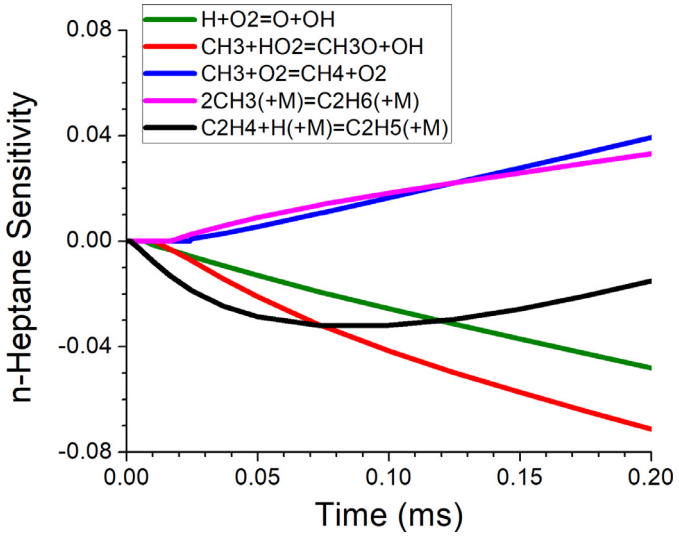

Fig. 17. Sensitivity analysis results for n-heptane at $T = 1235$ K and $P = 1.8$ atm. For the first 100 μs, the reaction $C_2H_4 + H\ (+M) = C_2H_5\ (+M)$ is the dominant reaction controlling n-heptane decay (simulations using detailed LLNL n-heptane mechanism [11] with Chemkin Pro [51]).

The CO_2 laser was tuned to the P14 line at 10.532 μm which coincides with a largely interference free absorption feature of ethylene from the HITRAN and PNNL databases [48,49]. The absorption cross section of ethylene is temperature dependent and has been measured by Pila et al. [40] and Ren et al. [50] at this wavelength. The ethylene absorption cross section was verified in our setup (using ethylene/Ar shock heated mixtures) for a temperature range of 1022–1735 K over pressures ranging from 1.4 to 1.9 atm. According to Ren et al., the cross section is observed to have a weak pressure dependence for pressures above 1.2 atm [50]. A purely mathematical model of the cross section in this temperature range was fit to the data as shown in Fig. 3.

The fit is described by Eq. (2) as follows:

$$\sigma(T) = A\left(\frac{T}{1000}\right)^B, \ \frac{m^2}{mol}, \tag{2}$$

where $A = 13.27\ m^2/mol$ and $B = -2.00$. This fit was used to calculate the ethylene absorption cross section at each experimental temperature for experiments in the lower pressure range (around 1.6 atm). Estimated uncertainty in the cross section was 5% due to the combined uncertainties in temperature, pressure, initial mole fraction, path length, and measured absorbance signal. For higher pressure experiments, the cross section was not validated in the lab, but our measured data points were within 10% of the model proposed in Ren et al., as shown in Fig. 4, so their fit was used for experiments with pressures ranging from 4.8 to 6.2 atm [50]. The fit is described by Eq. (3):

$$\sigma(T,P) = \left(a_0 + a_1 \exp\left(-\frac{T}{b_1}\right) + a_2 \exp\left(-\frac{T}{b_2}\right)\right)\left(c_0 + c_1 P^{d_1}\right), \ \frac{m^2}{mol} \tag{3}$$

with $a_0 = 4.8$, $a_1 = 383.7$, $a_2 = 103.5$, $b_1 = 183.0$, $b_2 = 378.8$, $c_0 = 0.82$, $c_1 = 0.2$, and $d_1 = -0.1$.

The major combustion species were estimated using the detailed LLNL n-heptane mechanism [11] for $T = 1235$ K and $P = 1.8$ atm using Chemkin Pro [51] for a $\varphi = 2.0$, 2% mixture of n-heptane and oxygen in an argon bath (results shown in Fig. 5). The main potential interfering species at the CO_2 laser wavelength are other alkenes, such as propene and butenes. Water, while also a major combustion product, has negligible absorption at the wavelength used in this study, and therefore is not an interfering species. These other alkenes also have significantly lower absorption cross sections (PNNL [49]) at 10.532 μm, as shown in Fig. 6. Additionally, as shown in Fig. 5, these species are produced in significantly lower concentrations than ethylene, and combined with their weak absorption cross sections do not interfere significantly with ethylene concentration time-history measurements, with an estimated interference of 0.5%. Thus, the measurement of ethylene mole fraction was performed at 10.532 μm and the measured absorbance was assumed to be completely due to the presence of ethylene.

2.3.2. n-Heptane laser scheme

A continuous wave distributed feedback interband cascade laser (Nanoplus DFB ICL) at 3.403 µm was used to measure n-heptane time-histories via a direct absorption spectroscopy scheme similar to that used to measure ethylene (Fig. 2) and is discussed in detail in Koroglu et al. [43,46]. Note that methane also strongly absorbs at this wavelength and is formed during the combustion of n-heptane. However, at early times (under 100 μs) methane concentration is negligible compared to that of n-heptane, as shown in Fig. 7. The predicted absorption for each species is shown in Fig. 8, in which we used the measured cross-section for n-heptane absorption and methane absorption cross section at 1235 K from HITRAN [48] in conjunction with the simulated mole fraction to calculate the absorbance signal. Even at 100 μs, the contribution from methane absorption to the overall signal is less than 1%. Because of the relatively low methane concentration, the absorption at this wavelength for early times can be considered to be due primarily to n-heptane. It is clear from Fig. 8 that the initial decay rate of n-heptane can be measured using the current strategy.

The temperature dependent n-heptane absorption cross section at 3.403 µm was measured over the range of shock tube temperatures by measuring the absorbance signal immediately after the reflected shock wave (assuming no n-heptane decomposition at time zero). A linear fit was used to determine the n-heptane absorption cross section at 3.4 μm for each of the experimental temperatures. The measured cross section and best fit line are shown in Fig. 9. The best fit line is described by Eq. (4) where

$A = -0.037\ m^2/mol\,K$ and $B = 79.3\ m^2/mol$.

$$\sigma(T) = AT + B, \ \frac{m^2}{mol} \tag{4}$$

2.4. Chemkin Pro simulations of shock tube with chemical kinetic mechanism

Experimental data were compared to 0-D chemical kinetics simulations performed with Chemkin Pro [51] using the LLNL detailed n-heptane mechanism [11]. It is important to use the correct thermodynamic assumptions while modeling shock tube data [52–54]. In order to model the experiments accurately, thermodynamic assumptions of constant pressure and internal energy or constant volume and internal energy were used, depending on which better fit the measured pressure trace of each experiment. Some experiments behaved as constant pressure systems due to the use of driver inserts, while others behaved as constant volume systems, as shown in Fig. 10. The model which best fit the pressure trace was selected for each simulation. A percent pressure rise per millisecond modeling approach was not used, because the experiments which had a pressure rise closely matched the pressure profile of a constant volume thermodynamic assumption.

For both constant pressure and constant volume simulations, the predicted temperature of the reacting mixture was found to vary significantly over the course of the experiment. An example of this is shown in Fig. 11, which shows the simulated T_5 for a constant pressure reacting system for $\varphi = 2.0$, 2% n-heptane/oxygen/argon mixture with $P_5 = 1.8$ atm.

According to the chemical kinetic model, the temperature varies by over 30% during the course of the experiment. This temperature variance leads to a change in the ethylene cross section and in the number density, contributing to a change in the observed absorbance, as described by Eq. (1). Thus, in order to compare the measured ethylene mole fractions to simulation results, the expected absorbance signal that would be measured given the chemical kinetic simulated mole fraction, temperature, and pressure was calculated and directly compared with the measured absorbance of the CO_2 laser. The simulated absorbance was calculated and compared to the measured absorbance, rather than the other way around, because the temperature during the experiment is not directly measured as a function of time and is only known accurately at the beginning of the experiment as a result of the ideal shock relations.

This calculation was repeated with two different sets of assumptions (Rules 1 and 2) in order to compare the impact of the temperature and pressure variance. The first procedure (Rule 1) assumed mole fraction, temperature, and pressure (and thus ethylene absorption cross section) are all functions of time and calculated expected absorbance at each time step based on the instantaneous simulated *T*, *P*, and mole fraction. The second set of assumptions (Rule 2) was that temperature and pressure (and thus ethylene absorption cross section) were constant and equal to their initial T_5 and P_5 values, and that the only variance in observed absorbance was due to the change in ethylene mole fraction (as is done in typical shock tube experiments). This was equivalent to calculating the mole fraction from the measured absorbance trace, making the same assumptions about temperature and pressure.

The current data analysis procedure leads to an inherent coupling in the output results (temperature, pressure, and mole fraction) of the model. While this makes it more difficult to attribute differences between the modeled and measured results to uncertainties in the reaction rates or improper thermodynamic assumptions, the strategy outlined in this section (Rules 1 and 2) provides a better check on the accuracy of the chemical kinetic models because it accounts for the temperature influence on the absorption cross section and number density, which influence the measured absorbance. Without accounting for these effects, variations in measured signal may be erroneously attributed solely to fluctuation in mole fraction, which would lead to improper optimization of chemical kinetic models.

3. Results and discussions

Experiments were performed over a range of temperatures from $T_5 = 1066$ to 1502 K at equivalence ratios of $\varphi = 2.0$ and 3.0, over pressure ranges P_5 from 1.4 to 6.2 atm (summarized in Table 2.) Uncertainty in initial mole fractions is ± 1.5% of the reported value.

3.1. Ethylene measurements

3.1.1. Ethylene time-histories

Select traces from the experimental sets are shown in Fig. 12. The measured absorbance is plotted along with the modeled absorbance using the two sets of assumptions (Rules 1 and 2) of time dependent and constant pressure and temperature. Because the expected absorbance value is calculated from the simulated parameters, error bars are placed on the simulation traces. Estimated uncertainty in the simulated absorbance value is 10%, resulting from the combined uncertainties of pressure, temperature, path length, mole fraction, and absorbance cross section.

In general, Rule 1 yields better agreement with the measured absorbance time-histories than Rule 2. This difference is particularly prominent in the early stages of high temperature experiments for all equivalence ratios and pressures. The time-dependent assumption set (Rule 1) improves the agreement between the overall shape of the modeled and measured absorbance time-histories, as it accounts for thermodynamic effects of change in pressure and temperature that are neglected by the assumptions of Rule 2. For example, in Fig. 12(h), the maximum of the absorbance trace occurs immediately before the rapid consumption of ethylene, which is captured well by the assumptions of Rule 1. The time dependent *T, P* assumption (Rule 1) set also greatly improves agreement between simulated and measured absorbances for high pressure experiments for the $\varphi = 2.0$ mixture.

This improved agreement is not an unexpected result, as both the cross section and number density are dependent on *T* and *P*, and thus contribute to a change in measured absorbance. Furthermore, the inverse dependence of both number density and cross section on temperature lead to a compounding effect of change in absorbance with temperature, furthering the importance of considering its time varying effect.

Over the entire range of experimental conditions, there is generally good agreement between predicted and observed magnitude of absorbance. This suggests that with the thermodynamic assumptions selected to match each experiment, ethylene mole fraction and number density are well predicted by the LLNL kinetic mechanism.

As temperature increases at 1.7 atm, the time at which ethylene is rapidly consumed is overpredicted by the model for low pressure experiments for equivalence ratios of both $\varphi = 2.0$ and $\varphi = 3.0$, with the discrepancy becoming more pronounced as temperature increases. For high pressure experiments, the model tends to under predict the time of rapid ethylene consumption for both equivalence ratios at lower temperatures and better predicts the consumption time as temperature increases.

The uncertainty in the temperature behind the reflected shock leads to uncertainty in the time of rapid ethylene consumption. A simulation of the $\varphi = 2.0$, $P_5 = 1.7$ atm experiment was performed with post reflected shock temperatures changed by 2% in either direction in order to estimate its effect on the observed chemical kinetics. The results are shown in Fig. 13.

3.1.2. Peak ethylene absorbance

The peak ethylene absorbance, defined as the maximum value of the absorbance signal, was obtained for each experiment and is shown in Fig. 14.

The peak ethylene absorbance was compared to results from simulations using both Rules 1 and 2, as described above. In general, the modeled peak ethylene absorbance as calculated with Rule 1 agreed better with the experimentally measured results, except for high pressure combustion of the $\varphi = 3.0$ mixture at temperatures above 1300 K. For both $\varphi = 2.0$ and 3.0 mixtures, the model tends to under predict peak ethylene absorbance for the low-pressure experiments, and tends to overpredict peak ethylene absorbance for high pressure experiments. For the $\varphi = 2.0$ experiments at $P \cong 5.9$ atm (Fig. 14(b)), the experimental peak ethylene absorbance shows a weak linear negative temperature dependence. This is matched well by the chemical kinetic model analyzed using Rule 1, while the temperature dependence is exaggerated when analyzed using Rule 2. It should be noted that because the peak ethylene absorbance is defined as the maximum value over the course of the experiment, the times at which the maxima occur for the measured and molded results in a single experiment vary.

3.2. n-Heptane initial decay rates

The initial decay rate of n-heptane was measured for the first 100 μs of the experiment, when methane concentration is negligible (as explained earlier in Fig. 8). Figure 15 provides the measured and predicted absorbance of the 3.4 µm laser due to n-heptane absorption, calculated with the same two sets of assumptions (Rules 1 and 2) as described before. Only traces from low pressure experiments are shown, because the absorbance signal was saturated for higher pressure experiments, owing to the combined high number density and absorption cross section.

At lower temperatures, initial n-heptane decay profile is well predicted by the LLNL mechanism for both equivalence ratios studied. As temperature increases, the initial decay rate is overpredicted by the model. It should be noted that both Rules 1 and 2 yield similar results for the predicted absorbance value (this is not unexpected, as the temperature change is small over the first 100 µs of the experiment).

3.3. Sensitivity analysis

In order to understand the oxidation of n-heptane, a detailed linear sensitivity analysis was performed using the detailed LLNL n-heptane mechanism [11] with Chemkin Pro [51], where the sensitivity coefficient (S) for ith reaction rate (k_i) for a species is defined as:

$$S(X_{species}, k_i, t) = \left\{ \frac{dX_{species}(t)}{dk_i} \right\} \left\{ \frac{k_i}{X_{species}(t)} \right\} \quad (5)$$

The results of the sensitivity analysis for the ethylene formation during fuel rich n-heptane combustion for a 2% n-heptane in argon bath mixture at $\varphi = 2.0$ for $T = 1235$ K and $P = 1.8$ atm is shown in Fig. 16. In general ethylene concentration is strongly affected by the HO_2 chemistry. The reaction strongly dominating the formation of ethylene for the first 200 μs is $C_2H_4 + H(+M) = C_2H_5 + HO_2$ (Rxn. 1). At these initial conditions for all temperatures studied, the predicted and measured ethylene concentration time-histories were in good agreement (as seen in Fig. 12) suggesting that the rate constant values used in the mechanism are probably the right ones. After the initial 200 μs, the main reaction responsible for ethylene formation is $C_2H_5 + O_2 = C_2H_4 + HO_2$ (Rxn. 2). Note that the agreement with the data is worsened at these conditions in some cases (e.g., Fig. 12(f)) and there is disagreement between the rate constant values used in the mechanism and in the literature recommended values [55,56]. Though improving the mechanism performance by adopting different reaction rates for Rxn. 2 is possible, updating the literature kinetic mechanism is outside the scope of the present work and must be done carefully. Current measurements highlight the deficiency in our knowledge of the chemical kinetics of n-heptane (an important reference fuel which is also widely studied in the literature) under fuel rich conditions. Most importantly, there exists no direct experimental determination of these crucial reaction rates (Rxns. 1 and 2) for the conditions used in this study.

A n-heptane sensitivity analysis was also performed to determine the key reactions dictating its initial breakdown, as shown in Fig. 17. In general, the methyl radical chemistry plays a crucial role in n-heptane decomposition. For the first 100 μs, the reaction $C_2H_4 + H\ (+M) = C_2H_5\ (+M)$ was found to be the dominant reaction controlling n-heptane decay. However, a recent study measuring the rate of this reaction reported an average uncertainty of 25% [57]. The rate coefficient for this reaction was thus increased and decreased by 25% in order to see the changes in the predicted initial decay rate of n-heptane. No significant change was observed in the predicted ethylene time-history with the changed reaction rates. This is expected because 25% change in rate coefficient is not a significant deviation to cause difference in predictions and because of the weak sensitivity coefficient ($S < 0.04$). A recent calculation of the rate coefficient was made by Miller and Klippenstein and is within a factor of 3 of the LLNL reaction rate [58]. Additional measurements of CH_3 radical time-histories would help in identifying the reasons behind the disagreement between predicted and measured n-heptane time-histories shown in Fig. 15. However, the current data would serve as a validation target for future refinement of the LLNL kinetic model.

Current measurements reveal that there is a need to better understand fuel rich oxidation even for well-studied reference fuel components (e.g., n-heptane) and that caution must be exercised while using heptane kinetic mechanisms outside their validation limit. Effort is currently underway in our laboratory to expand the ranges of current experimental measurements to other T, P, and concentration regions. Additional intermediate species time-histories (e.g., CO, CH_3, HCHO, CH_4, C_3H_6, etc.) will also be targeted using existing and new laser absorption schemes.

4. Conclusions

In this study, we provided the first ethylene and n-heptane time-histories using laser absorption spectroscopy for fuel-rich $\varphi = 2.0$ and 3.0 mixtures of 2% n-heptane and oxygen in argon at temperatures of $1066 < T_5 < 1502$ K over two pressure ranges from 1.4 to 1.9 atm and from 4.8 to 6.2 atm behind reflected shock waves. Concentration time-histories were compared against chemical kinetic simulations (using the Lawrence Livermore National Lab (LLNL) detailed n-heptane reaction mechanism [11]) by calculating the predicted absorbance due to a species rather than directly calculating the concentration time-history from measurements. In doing so, the effects of time dependent temperature and pressure variation, and their subsequent effects on absorption cross section and number density, were properly taken into account in 0-Dimensional shock tube simulations. Two sets of assumptions were used when calculating simulated absorbance, with one set taking into account the time-dependence of temperature and pressure, and the other assuming a constant temperature and pressure. Good agreement was found between predicted and measured absorbance time histories from ethylene absorption, with excellent agreement at early times. The time-dependent temperature and pressure assumption set yielded better agreement than the constant temperature and pressure assumption set. Initial n-heptane time histories agreed well for lower temperatures, but the model overpredicted rate of fuel consumption as temperature increased for both equivalence ratios studied. Sensitivity analysis revealed the crucial reactions that are impor-

tant for fuel rich n-heptane oxidation under current experimental conditions. Detailed investigation of the kinetic pathways and reaction rates may lead to improved predictions for rich mixtures and higher temperatures. The current data will serve as a crucial validation target for developing and refining n-heptane kinetic mechanisms – an important reference fuel for the combustion of real fuels.

Notice of Copyright

Acknowledgments

This material is based upon work supported by the National Science Foundation Graduate Research Fellowship Program under Grant no. 1144246. Donors of the American Chemical Society Petroleum Research Fund and the Defense Threat Reduction Agency (Grant number: HDTRA1-16-1-0009) are acknowledged for partial financial support. Any opinions, findings, and conclusions or recommendations expressed in this material are those of the author(s) and do not necessarily reflect the views of the National Science Foundation. J.L. acknowledges funding provided by the National Aeronautics and Space Administration Florida Space Grant Consortium. The authors thank assistance from Owen Pryor, Leigh Nash, and Sam Barak during UCF shock tube experiments. The Oak Ridge National Laboratory research was sponsored by the U.S. Department of Energy, Office of Energy Efficiency and Renewable Energy, Vehicle Technologies Office, with Gurpreet Singh as the Program Managers.

Supplementary materials

Supplementary material associated with this article can be found, in the online version, at doi:10.1016/j.combustflame.2017.07.016.

References

[1] D.K. Marsh, A.K. Voice, Quantification of knock benefits from reformate and cooled exhaust gas recirculation using a Livengood–Wu approach with detailed chemical kinetics, Int. J. Engine Res. 1468087416666728.
[2] A.A. Quader, J.E. Kirwan, M.J. Grieve, Engine performance and emissions near the dilute limit with hydrogen enrichment using an on-board reforming strategy, 2003 Report No. 2003-01-1356, SAE Technical Paper.
[3] Corporate Average Fuel Economy (CAFE) for MY 2017-MY 2025 Passenger cars and light trucks U.S. department of transportation national highway traffic safety administration (2012) available at: http://www.nhtsa.gov/fuel-economy.
[4] V.B. Kalaskar, J.P. Szybist, D.A. Splitter, J.A. Pihl, Z. Gao, C.S. Daw, In-cylinder reaction chemistry and kinetics during negative valve overlap fuel injection under low-oxygen conditions, ASME Internal Combustion Engine Division Fall Technical Conference, Dearborn, Michigan (2013).
[5] L. Manofsky, D. Assanis, A. Babajimopoulos, Bridging the gap between HCCI and SI: spark-assisted compression ignition, SAE Int. J. Engines (2011) Paper No: 2011-01-1179.
[6] T. Alger, B. M., Dedicated EGR: a new concept in high efficiency engines, SAE Int. J. Engines 2 (2009) 620–631 Paper No: 2009-01-0694.
[7] V. Kalaskar, J.P. Szybist, D. Splitter, J. Pihl, Z. Gao, C.S. Daw, In-cylinder reaction chemistry and kinetics during negative valve overlap fuel injection under low-oxygen conditions, Proceedings of ASME 2013 Internal Combustion Engine Division Fall Technical Conference, Dearbon, MI (2013), pp. 1–15.
[8] J.P. Szybist, D. Steeper, D. Splitter, V. Kalaskar, J. Pihl, S. Daw, Negative valve overlap reforming chemistry in low-oxygen environments, SAE 2014-01-1188, (2014).
[9] M. Mehl, H. Curran, W. Pitz, C. Westbrook, Chemical kinetic modeling of component mixtures relevant to gasoline, European Combustion Meeting (2009).
[10] M. Mehl, W.J. Pitz, M. Sjöberg, J. Dec, Detailed kientic modeling of low-temperature heat release for PRF fuels in an HCCI Engine, SAE Technical Paper No: 2009-01-1806, (2009).
[11] M. Mehl, W.J. Pitz, C.K. Westbrook, H.J. Curran, Kinetic modeling of gasoline surrogate components and mixtures under engine conditions, Proc. Combust. Inst. 33 (2011) 193–200.
[12] D.A. Sheen, W. Tsang, A comparison of literature models for the oxidation of normal heptane, Combust. Flame 161 (2014) 1984–1992.
[13] J. Zhang, S. Niu, Y. Zhang, C. Tang, X. Jiang, E. Hu, Z. Huang, Experimental and modeling study of the auto-ignition of n-heptane/n-butanol mixtures, Combust. Flame 160 (2013) 31–39.
[14] S.H. Pyun, W. Ren, D.F. Davidson, R.K. Hanson, Methane and ethylene time-history measurements in n-butane and n-heptane pyrolysis behind reflected shock waves, Fuel 108 (2013) 557–564.
[15] E. Mancaruso, B.M. Vaglieco, An experimental comparison of n-heptane, RME and diesel fuel on combustion characteristics in a compression ignition engine, Fuel Process. Technol. 107 (2013) 44–49.
[16] Y.W.M. Bolla, K. Boulouchos, G. Borghesi, E. Mastorakos, Soot formation modeling of n-heptane sprays under diesel engine conditions using the conditional moment closure approach, Combust. Sci. Technol. 185 (5) (2013) 766–793.
[17] D. Darcy, M. Mehl, J.M. Simmie, J. Würmel, W.K. Metcalfe, C.K. Westbrook, W.J. Pitz, H.J. Curran, An experimental and modeling study of the shock tube ignition of a mixture of n-heptane and n-propylbenzene as a surrogate for a large alkyl benzene, Proc. Combust. Inst. 34 (2013) 411–418.
[18] D.M.A. Karwat, S.W. Wagnon, M.S. Wooldridge, C.K. Westbrook, On the combustion chemistry of n-heptane and n-butanol blends, J. Phys. Chem. A 116 (2012) 12406–12421.
[19] Y. Zhang, A.L. Boehman, Oxidation of 1-butanol and a mixture of n-heptane/1-butanol in a motored engine, Combust. Flame 157 (2010) 1816–1824.
[20] D.F. Davidson, Z. Hong, G.L. Pilla, A. Farooq, R.D. Cook, R.K. Hanson, Multi--species time-history measurements during n-heptane oxidation behind reflected shock waves, Combust. Flame 157 (2010) 1899–1905.
[21] S.S. Vasu, D.F. Davidson, R.K. Hanson, OH time-histories during oxidation of n-heptane and methylcyclohexane at high pressures and temperatures, Combust. Flame 156 (2009) 736.
[22] Z. Hong, D.F. Davidson, S.S. Vasu, R.K. Hanson, The effect of oxygenates on soot formation in rich heptane mixtures: a shock tube study, Fuel 88 (2009) 1901–1906.
[23] P. Dagaut, C. Togbe´, Experimental and modeling study of the kinetics of oxidation of butanol−n-heptane mixtures in a jet-stirred reactor, Energy Fuels 23 (2009) 3527–3535.
[24] J. Herzler, M. Fikri, K. Hitzbleck, R. Starke, C. Schulz, P. Roth, G.T. Kalghatgi, Shock-tube study of the autoignition of n-heptane/toluene/air mixtures at intermediate temperatures and high pressures, Combust. Flame 149 (2007) 25–31.
[25] H.K. Ciezki, G. Adomeit, Shock-tube investigation of self-ignition of n-heptane–air mixtures under engine relevant conditions, Combust. Flame 93 (1993) 421–433.
[26] C.K. Westbrook, J. Warnatz, W.J. Pitz, A detailed chemical kinetic reaction mechanism for the oxidation of iso-octane and n-heptane over an extended temperature range and its application to analysis of engine knock, Symp. (Int.) Combust. 22 (1989) 893–901.
[27] H. Curran, W. Pitz, C. Westbrook, NC7_2b Mechanism, UCRL-WEB-204236 Release, 2004.
[28] D. Davidson, J. Herbon, D. Horning, R. Hanson, OH concentration time histories in n-alkane oxidation, Int. J. Chem. Kinet. 33 (2001) 775–783.
[29] D.F. Davidson, M.A. Oehlschlaeger, R.K. Hanson, Methyl concentration time-histories during iso-octane and n-heptane oxidation and pyrolysis, Proc. Combust. Inst. 31 (2007) 321–328.
[30] B.M. Gauthier, D.F. Davidson, R.K. Hanson, Shock tube determination of ignition delay times in full-blend and surrogate fuel mixtures, Combust. Flame 139 (2004) 300.
[31] B. Sirjean, E. Dames, D. Sheen, X. You, C. Sung, A. Holley, F. Egolfopoulos, H. Wang, S. Vasu, D. Davidson, A hightemperature chemical kinetic model of n-alkane oxidation, JetSurF version 0.2, JetSurF version 1, (2009).
[32] J.M. Smith, J.M. Simmie, H.J. Curran, Autoignition of heptanes; experiments and modeling, Int. J. Chem. Kinet. 37 (2005) 728–736.
[33] M.F. Campbell, S. Wang, C.S. Goldenstein, R.M. Spearrin, A.M. Tulgestke, L.T. Zaczek, D.F. Davidson, R.K. Hanson, Constrained reaction volume shock tube study of n-heptane oxidation: ignition delay times and time-histories of multiple species and temperature, Proc. Combust. Inst. 35 (2015) 231–239.
[34] A. Tekawade, G. Kosiba, M.A. Oehlschlaeger, Time-resolved carbon monoxide measurements during the low- to intermediate-temperature oxidation of n-heptane, n-decane, and n-dodecane, Combust. Flame 173 (2016) 402–410.
[35] H. Wang, R. Deneys Reitz, M. Yao, B. Yang, Q. Jiao, L. Qiu, Development of an n-heptane-n-butanol-PAH mechanism and its application for combustion and soot prediction, Combust. Flame 160 (2013) 504–519.
[36] J.B. Randazzo, C.J. Annesley, K. Bell, R.S. Tranter, A shock tube laser schlieren study of cyclopentane pyrolysis, Proc. Combust. Inst., doi:http://dx.doi.org/10.1016/j.proci.2016.05.038 (2016).

[37] S.S. Vasu, S.M. Sarathy, On the high-temperature combustion of n-butanol: shock tube data and an improved kinetic model, Energy Fuels 27 (2013) 7072–7080.
[38] C. Lee, S. Vranckx, K.A. Heufer, S.V. Khomik, Y. Uygun, H. Olivier, R.X. Fernandes, On the chemical kinetics of ethanol oxidation: shock tube, rapid compression machine and detailed modeling study, Z. Phys. Chem. 226 (2012) 1–27.
[39] Z.E. Loparo, J.G. Lopez, S. Neupane, W.P. Partridge, K.L. Vodopyanov, S.S. Vasu, Time-resolved measurements of intermediate concentrations in fuel-rich n-heptane oxidation behind reflected shock waves, ASME Trubo Expo 2017: Turbomachinery Technical Conference and Exposition, Charlotte, North Carolina, USA (2017), pp. GT2017–G63344.
[40] G.L. Pilla, D.F. Davidson, R.K. Hanson, Shock tube/laser absorption measurements of ethylene time-histories during ethylene and n-heptane pyrolysis, Proc. Combust. Inst. 33 (2011) 333–340.
[41] H.-P.S. Shen, J. Steinberg, J. Vanderover, M.A. Oehlschlaeger, A shock tube study of the ignition of n-heptane, n-decane, n-dodecane, and n-tetradecane at elevated pressures, Energy Fuels 23 (2009) 2482–2489.
[42] J. Herzler, L. Jerig, P. Roth, Shock tube study of the ignition of lean n-heptane/air mixtures at intermediate temperatures and high pressures, Proc. Combust. Inst. 30 (2005) 1147–1153.
[43] B. Koroglu, O. Pryor, J. Lopez, L. Nash, S.S. Vasu, Shock tube ignition delay times and methane time-histories measurements during excess CO_2 diluted oxy-methane combustion, Combust. Flame 164 (2016) 152–163.
[44] O.M. Pryor, S. Barak, B. Koroglu, E. Ninnemann, S.S. Vasu, Measurements and interpretation of shock tube ignition delay times in highly CO_2 diluted mixtures using multiple diagnostics, Combust. Flame 180 (2017) 63–76.
[45] G. Barari, O. Pryor, B. Koroglu, J. Lopez, L. Nash, S.M. Sarathy, S.S. Vasu, High temperature shock tube experiments and kinetic modeling study of diisopropyl ketone ignition and pyrolysis, Combust. Flame 177 (2017) 207–218.
[46] B. Koroglu, S.S. Vasu, Measurements of propanal ignition delay times and species time histories using shock tube and laser absorption, Int. J. Chem. Kinet. 48 (2016) 679–690.
[47] H. Mark, The interaction of a reflected shock wave with the boundary layer in a shock tube, National Advisory Committee for Aeronautics, 1958.
[48] L.S. Rothman, I.E. Gordon, Y. Babikov, A. Barbe, D. Chris Benner, P.F. Bernath, M. Birk, L. Bizzocchi, V. Boudon, L.R. Brown, A. Campargue, K. Chance, E.A. Cohen, L.H. Coudert, V.M. Devi, B.J. Drouin, A. Fayt, J.M. Flaud, R.R. Gamache, J.J. Harrison, J.M. Hartmann, C. Hill, J.T. Hodges, D. Jacquemart, A. Jolly, J. Lamouroux, R.J. Le Roy, G. Li, D.A. Long, O.M. Lyulin, C.J. Mackie, S.T. Massie, S. Mikhailenko, H.S.P. Müller, O.V. Naumenko, A.V. Nikitin, J. Orphal, V. Perevalov, A. Perrin, E.R. Polovtseva, C. Richard, M.A.H. Smith, E. Starikova, K. Sung, S. Tashkun, J. Tennyson, G.C. Toon, V.G. Tyuterev, G. Wagner, The HITRAN2012 molecular spectroscopic database, J. Quant. Spectrosc. Radiat. Transf. 130 (2013) 4–50.
[49] S.W. Sharpe, T.J. Johnson, R.L. Sams, P.M. Chu, G.C. Rhoderick, P.A. Johnson, Gas-phase databases for quantitative infrared spectroscopy, Appl. Spectrosc. 58 (2004) 1452–1461.
[50] W. Ren, D.F. Davidson, R.K. Hanson, IR laser absorption diagnostic for C_2H_4 in shock tube kinetics studies, Int. J. Chem. Kinet. 44 (2012) 423–432.
[51] CHEMKIN-PRO 15131, Reaction design, San Diego, CA, 2013.
[52] J. Melguizo-Gavilanes, L. Bauwens, A comparison between constant volume induction times and results from spatially resolved simulation of ignition behind reflected shocks: implications for shock tube experiments, Shock Waves 23 (2013) 221–231.
[53] M. Chaos, F.L. Dryer, Chemical-kinetic modeling of ignition delay: considerations in interpreting shock tube data, Int. J. Chem. Kinet. 42 (2010) 143–150.
[54] D.F. Davidson, R.K. Hanson, Interpreting shock tube ignition data, Int. J. Chem. Kinet. 36 (2004) 510.
[55] D. Baulch, C. Cobos, R. Cox, C. Esser, P. Frank, T. Just, J. Kerr, M. Pilling, J. Troe, R. Walker, Evaluated kinetic data for combustion modelling, J. Phys. Chem. Ref. Data 21 (1992) 411–734.
[56] J.W. Bozzelli, A.M. Dean, Chemical activation analysis of the reaction of ethyl radical with oxygen, J. Phys. Chem. 94 (1990) 3313–3317.
[57] X. Yang, R.S. Tranter, High-temperature dissociation of ethyl radicals and ethyl iodide, Int. J. Chem. Kinet. 44 (2012) 433–443.
[58] J.A. Miller, S.J. Klippenstein, The $H + C_2H_2$ (+M) [right left arrows] C_2H_3 (+M) and $H + C_2H_2$ (+M) [right left arrows] C_2H_5 (+M) reactions: electronic structure, variational transition-state theory, and solutions to a two-dimensional master equation, Phys. Chem. Chem. Phys. 6 (2004) 1192–1202.